Journal of the Korean Electrochemical Society
Vol. 10, No. 2, 2007, 116-125

Synthesis and Characterisation of Mixed Conducting Perovskite Type Oxide and Its Electrochemical Application to Electrode Material for Solid Oxide Fuel Cell

Yu-Mi Kim, Su-Il Pyun*, Gyoung-Ja Lee, and Ju-Sik Kim

Department of Materials Science and Engineering, Korea Advanced Institute of Science and Technology, 373-1 Guseong-Dong, Yuseong-Gu, Daejeon 305-701, Republic of KOREA

(Received April 6, 2007 : Accepted April 16, 2007)

Abstract : This article is concerned with synthesis, characterisation and electrochemical application of the mixed conducting perovskite type oxide to electrode materials for solid oxide fuel cell. First, this review provides a comprehensive survey of the various synthetic methods such as solid state reaction, Pechini, glycine nitrate process and sol-gel methods for the preparation of perovskite type oxide powders. Subsequently, the electrical and microstructural properties of the mixed conducting oxides were discussed in detail. Finally, as electrochemical applications of the mixed conducting perovskite type oxides to electrode materials for solid oxide fuel cell, fundamentals of theoretical ac-impedance model for porous mixed conducting electrodes were introduced. Furthermore, the ac-impedance behaviour of porous and dense mixed conducting electrodes prepared by various synthetic methods was discussed.

Keywords : Mixed conducting oxide, Perovskite structure, Solid oxide fuel cell, Ac-impedance spectra, Oxygen reduction reaction.

1. Introduction

A material which exhibits both electronic and ionic conductivities is generally referred to as a mixed ionic/electronic conductor (MIEC). Among various MIECs, perovskite type oxides have attracted much attention in many areas of solid state electrochemical devices including electrodes for sensors,[1,2] solid oxide fuel cells (SOFCs),[3-8] oxygen separation membranes[9-11] and catalytic membrane reactors[12,13] due to their higher ionic/electronic conductivities. In particular, the perovskite type oxide has been widely used as cathode material for SOFC due to its fast exchange of oxygen between the gaseous phase and the oxide, good ionic/electronic conductivities and relatively low cost.

It has been reported that the mixed ionic/electronic conductivities of perovskite type oxides are greatly affected by cation content,[14-17] temperature[15,18-21] and oxygen partial pressure.[22-26] Especially, the cation content of the mixed conducting oxide significantly influences the electrical conductivity, since cation content can change the oxygen stoichiometry of the oxide through the formation of oxygen vacancy and charge compensation of transition metal cation.

The MIECs with perovskite structure are prepared by various methods such as solid state reaction,[27-32] Pechini,[33-37] glycine nitrate process[38-40] and sol-gel methods[41-43] in order to enhance the performance of cathodic material, reducing its cost as much as possible. The geometrical properties of the sintered cathodic electrode are greatly affected by the characteristics of the powder during the synthetic process.[44] Under these circumstances, for a more exact analysis of oxygen reduction on the MIECs, the relationship should be considered between the powder synthetic methods and the microstructural properties of the electrode such as particle size, porosity and pore size.

In this respect, this article provides a comprehensive survey of synthetic methods and electrical/microstructural properties of the MIECs with perovskite structure. Furthermore, as electrochemical applications of the mixed conducting perovskite oxides to electrode materials for SOFC, the theoretical ac-impedance model for porous MIECs was introduced. And then, the ac-impedance behaviour of porous and dense mixed conducting electrodes with various powder synthetic methods was discussed.

2. Synthesis of the mixed conducting oxides with perovskite structure

Powder synthesis plays an important role in determining the powder characteristics such as particle size, particle size distribution, pore size and porosity which affect the electrochemical properties of the electrode. There are many chemical methods for the synthesis of powders: One is the conventional method using solid state reaction and the other is the method using liquid solution which includes Pechini, glycine nitrate process and sol-gel methods.

*E-mail: sipyun@webmail.kaist.ac.kr

2.1 Solid State Reaction (SSR) Method

SSR method is one of the chemical methods which are widely used for the preparation of ceramic powders.[29-32] Chemical reactions between solid starting materials, usually provided in the form of mixed powders, are commonly used for the production of complex oxide powders such as ferrites and silicates. Since mixed powders do not usually react together at room temperature, it is necessary to heat them to much higher temperatures, often 1273 to 1773 K, in order to obtain an appreciable reaction rate.

It is generally reported that the degree of reaction highly depends on the temperature at which SSR between starting oxides occurs. H. Nagamoto *et al.*[27] studied the dependence of SSR temperature on catalytic activities in $SrCeO_3$ catalysts by using X-ray diffraction (XRD), X-ray photoelectron spectroscopy (XPS) and temperature-programmed desorption (TPD) of CO gas. In their work, it was revealed that the surface area of the catalysts decreased with increasing SSR temperature, i.e., the number of reaction sites decreased with increasing temperature, whereas the reaction rate increased with increasing temperature. It is thus concluded that as SSR temperature increases, catalytic properties of catalysts are more improved.

It is well known that the preparation of powder by SSR method has advantages in reducing production cost and simplifying the complex preparation steps as compared with other methods. However, since SSR requires high temperature for complete reaction, the problems such as multi-phases and agglomerates have to be minimised in order to form homogeneous powders. The addition of catalyst can lower the SSR temperature. Also, the impurities of the powder can be removed by ultrasonic treatments or surface chemical treatments such as chlorine or fluorine addition.[45]

Since the powders can be easily agglomerated during the synthetic process using SSR method, a grinding step is always required to produce powders with smaller particle size and homogeneous particle size distribution. But grinding in ball mills commonly leads to the contamination of the powder with impurities. The difficulty in controlling the particle shape of powder is another practical problem of SSR method. Therefore, a great interest has been focused on the solution of the above practical problems.

2.2 Pechini and Glycine Nitrate Process (GNP) Methods

Among various methods for the preparation of the powders, most commonly used method is Pechini method which was first developed by Pechini[33] for the preparation of titanates and niobates for capacitor. Comparing to the SSR method, the powders with better characteristics and less impurities can be obtained by Pechini method. With slight modifications, it is also referred to as the citrate gel process or the amorphous citrate process which has been used for the preparation of a wide variety of oxide powders.[34-37]

Pechini synthesis proceeds by the following steps: (i) powders with metal ions are mixed in an aqueous solution with α-hydroxycarboxylic acids such as citric acid, (ii) these chelates can undergo polyesterification when heated with a polyhydroxy alcohol such as ethylene glycol, (iii) after removal of the excess solvent, a transparent solid resin containing the metals in solid solution is formed, and finally (iv) the resin is decomposed by heating to remove the organic constituents, leaving the desired ceramic composition as a residue.

When the aqueous solution with metal ions is heated, polyesterification occurs to remove the excess solvent and to form a solid resin. Since the formed resins have high porosity, high surface energy and high free energy, the final burning in Pechini method occurs at relatively lower temperatures as compared with that in SSR method. However, Pechini method is applicable to few kinds of initial reagents such as metal alkoxides, oxides and carbonates to prepare the solid resin. On the other hand, for GNP method, metal nitrates as well as the above reagents can be used as initial materials to prepare the precursor, and hence GNP method can easily produce various kinds of powders by mixing plentiful nitrates as compared with Pechini method.

The preparation of general oxide powders using GNP method is explained as follows: A highly viscous mass formed by evaporation of a solution containing metal nitrates and glycine is ignited to produce the powder. One of amino acids, glycine forms complexes with the metal ions in solution, which increases the solubility and prevents the precipitation of the metal ions as the water is evaporated. Glycine also plays another important role; it provides a fuel for the ignition step of the process as it is oxidised by the nitrate ions.[38-40]

Fig. 1 illustrates the histograms of chromite particle compositions of $La_xSr_{1-x}CrO_3$ powders for Pechini and GNP methods by using energy dispersive spectroscopy (EDS).[46] The powders prepared by Pechini method exhibited exten-

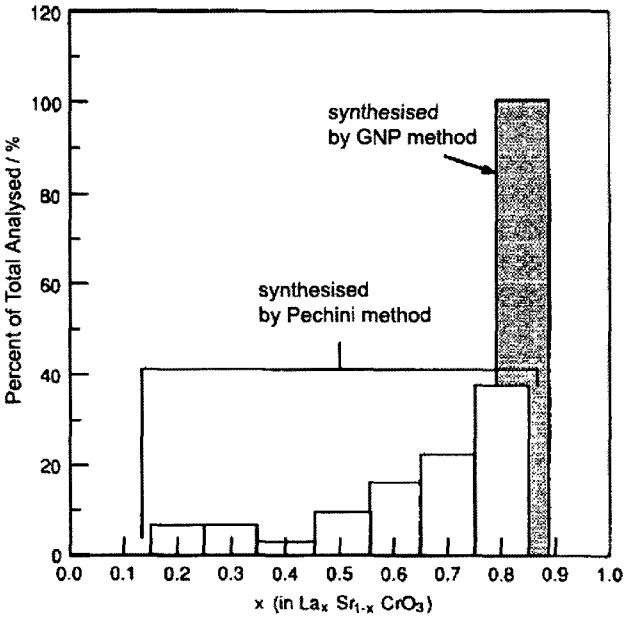

Fig. 1. Histograms of Cr particle composition obtained from the $La_xSr_{1-x}CrO_3$ electrode using energy dispersive spectroscopy (EDS). Open bars correspond to powder produced by Pechini method and the shaded bar corresponds to powder produced by glycine nitrate process (GNP) method. [46]

sive compositional variability, however, no intermediate-composition products were detected from the powders prepared by GNP method. From the above result, it is suggested that one of the advantages of GNP method is good chemical homogeneity of the final powders. Provided that none of the constituents are volatilised during the calcination step, the cation composition can be equivalent to that of the original solution.

Pechini combustion is sluggish and must be sustained for long times of external heating. This external heating enhances the grain growth, causing the decrease in specific surface area. On the other hand, GNP combustion occurs quite rapidly at high temperature above 1273 K, which leads to formation of the powders with high surface area, homogeneous distribution in composition and low levels of residual starting materials.

Under well-controlled conditions, very fine crystalline powders with nano-size can be obtained after ignition. In contrast to SSR method, grinding step which introduces the impurities into the powders is not required for GNP method. Accordingly, GNP method can offer a relatively inexpensive process for the preparation of very fine and chemically homogeneous powders. However, since the reactions during ignition are highly explosive, extreme care should be taken during the process.

2.3 Sol-Gel (SG) Method

In order to make up for the weak points of SSR method, SG method has been widely investigated since it provides an easy control of both microstructure and composition of oxide materials at low temperature.[41-43] Fig. 2 depicts the flow chart for the preparation of mixed conducting oxide powders by SG method. First, various metal nitrates are dissolved into absolute ethanol. The solution is then refluxed and stirred continuously for hours using a water bath, cooled to room temperature, and then concentrated to about 1/3 of its volume by evaporation of ethanol for hours in order to obtain sol-precursor. The sol-precursor is then stirred and dried for hours to get the gel. After ageing and calcination with slow heating rate, powders are finally obtained from the resulting gel.[28]

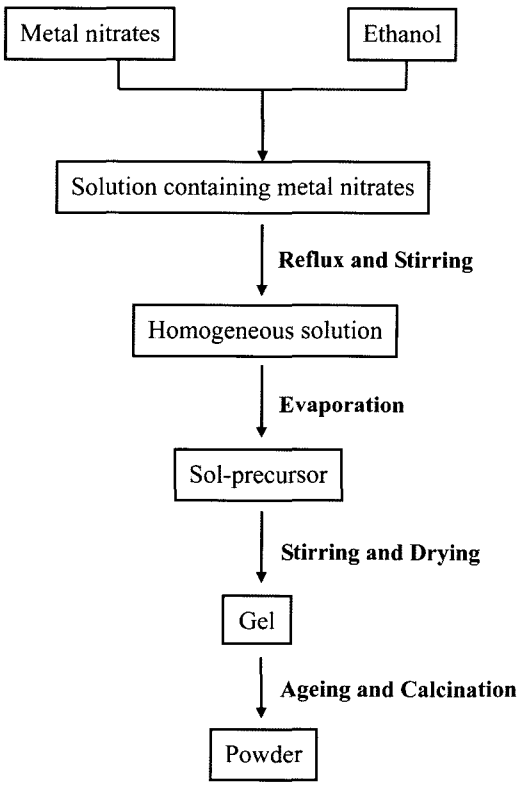

Fig. 2. Schematic diagram of the experimental procedure for the preparation of powders with perovskite structure using sol-gel (SG) method.

The main advantage of SG method is the formation of highly porous structures with large surface area which is useful for many applications. Furthermore, SG processing allows the easy control of the texture, composition, homogeneity, and microstructural properties of the resulting materials which influence the electrochemical properties of the MIECs. However, there also exist some disadvantages in SG method. The starting materials are fairly expensive. In addition, this method inevitably produces the crack and shrinkage on the resulting gel during the conventional drying step. Due to the above problems, the SG method has been used for the fabrication of small or thin articles such as films, fibers and powders.

3. Characterisation of Mixed Conducting Oxides with Perovskite Structure

3.1 Electrical Property

Recently, lanthanide cobaltites, $LnCoO_{3\pm\delta}$, have attracted much attention as promising candidates for mixed conducting electrodes due to their high ionic/electronic conductivities as well as noticeable electrochemical and catalytic activities in oxygen containing environments. Lanthanides such as La,[1,16] Pr[47,48] and Sm[47,49,50] are most commonly used as A-site cations, and Sr,[1,15,16,47,48] Ca[20,51,52] and Ba[50,53] dopants are usually doped in A-sites in order to improve the electrical properties of $LnCoO_{3\pm\delta}$ electrodes.

In general, the electrical property of MIECs mainly depends on the composition,[14-16] temperature[18-20] and oxygen partial pressure.[24] A common way to obtain electrodes with high ionic/electronic conductivities is to control the composition of A- and B-site cations. For instance, when Sr is doped in $LnCoO_{3\pm\delta}$, using Kröger-Vink notation, the defect chemistry of $Ln_{1-x}Sr_xCoO_{3-\delta}$ can be described by the following reactions:

$$O_o + 2Co_{Co}^{\cdot} \leftrightarrow \frac{1}{2}O_2 + V_O^{\cdot\cdot} + (2Co_{Co}) \quad (2)$$

$$[Co_{Co}^{\cdot}] + 2[V_O^{\cdot\cdot}] = [Sr'_{Ln}] \quad (3)$$

where O_o and Co_{Co} represent the O^{2-} and Co^{3+} cations, respectively, on regular sites; $Co^{\cdot}_{Co}$, the Co^{4+} cation on a Co^{3+} lattice position; $V_O^{\cdot\cdot}$, oxygen vacancy; Sr'_{Ln}, the substitution of Sr^{2+} for Ln^{3+} site. According to the International Union of Pure and Applied Chemistry (IUPAC) convention, $\leftrightarrow$ is the reaction in both the forward and reverse direction; =, the balancing of the equation; $\rightarrow$ represents the reaction in a single direction. Eq. (2) describes the oxygen exchange

between solid and gas phase via the annihilation of $V_O^{\cdot\cdot}$ and oxidation of Co^{3+} to Co^{4+}. Eq. (3) represents the overall electroneutrality condition. With ionic compensation ($V_O^{\cdot\cdot}$) and electronic compensation ($Co^{\cdot}_{Co}$) the electrical conductivity is influenced by A- and B-site content.

L.-W. Tai *et al.*[20] have investigated the electrical conductivity of $La_{1-x}Sr_xCo_{0.2}Fe_{0.8}O_{3-\delta}$ electrodes as a function of Sr contents ($0 \le x \le 0.4$), as shown in Fig. 3. Here, let us consider $La_{1-x}Sr_xBO_3$ (B = Co, Fe) electrodes with various Sr contents for simple analysis. According to the Kröger-Vink notation, the Sr^{2+} substitution for La^{3+} is electronically compensated by the oxidation of B^{3+} to B^{4+} cation as follows:

$$LaBO_3 \xrightarrow{SrO} La_{1-x}Sr'_xB_{1-x}B^{\cdot}_xO_3 \tag{4}$$

and/or ionically compensated by the formation of $V_O^{\cdot\cdot}$ as follows:

$$La_{1-x}Sr'_xB_{1-x}B^{\cdot}_xO_3 \leftrightarrow La_{1-x}Sr'_xB_{1-x+2\delta}B^{\cdot}_{x-2\delta}O_{3-\delta}[\delta V_O^{\cdot\cdot}] + \frac{\delta}{2}O_2 \tag{5}$$

In this respect, it is suggested from Fig. 3 that as Sr content increases at constant temperature, the electrical conductivity increases due to ionic/electronic compensation. V.V. Kharton *et al.*[17] also investigated the effect of B-site cation on the electrical properties such as ionic/electronic conductivities for $LaCo_{1-x-y}Fe_xNi_yO_3$ ($0.1 \le x \le 0.2$; $0.1 \le y \le 0.3$) electrodes. The increase in the nickel content increases the non-stoichiometry of the oxygen, thus causing the increase in the electrical conductivity.

G. Ch. Kostogloudis *et al.*[54] measured the electrical conductivity of $Pr_{1-x}Sr_xMnO_{3\pm\delta}$ electrodes with various Sr contents at 773, 873 and 973 K in air. From their work, it is observed that the conductivity increases with Sr content in all temperature cases, which is ascribed to the formation of $V_O^{\cdot\cdot}$ for ionic compensation and the oxidation of Mn^{3+} to Mn^{4+} for electronic compensation. The effect of A- and B-sites substitution on the electrical conductivity was also reported for $La_{1-x}Sr_xCo_{1-y}Fe_yO_{3-\delta}$[55] and $La_{1-x}Pb_xFeO_{3-\delta}$ electrodes.[29]

Temperature also affects the electrical conductivity of mixed conducting electrodes. It is well known that if the carrier concentration is constant, the Arrhenius plots of ln σT vs. $1/T$ are linear, as predicted by the following equation derived for the small polaron conduction:

$$\sigma = (C/T)\exp(-E_a/kT) \tag{6}$$

where C is the pre-exponential factor; k, the Boltzmann constant [eV K^{-1}]; σ, the electrical conductivity [S cm^{-1}]; T, the temperature [K]; E_a represents the activation energy [eV] for conduction. It is noted from Eq.(6) that the ionic/electrical conductivities are closely related to the temperature since the movement of ionic defects is a thermally activated hopping process, and the movement of electrons depends on temperature.

L.-W. Tai *et al.*[20] also studied the dependence of electrical conductivity on temperature for $La_{1-x}Sr_xCo_{0.2}Fe_{0.8}O_{3-\delta}$ electrodes with various Sr contents. As can be seen in Fig. 3, it was revealed that as temperature increased, the electrical conductivity gradually increased. On the other hand, from the thermogravimetric analysis (TGA), it was found that the oxygen content remained nearly constant in temperature range below 1073 K. This indicates that the dependence of ionic conductivity on temperature is weaker than that of electronic conductivity on temperature below 1073 K.

Furthermore, Y. Teraoka *et al.*[19] explored the effect of temperature on the ionic and electronic conductivities of $La_{0.6}Sr_{0.4}B_{0.8}Fe_{0.2}O_{3-\delta}$ (B = Fe, Co, Ni, Cu) electrodes using four-probe ionic dc technique and standard four-probe dc technique. From their work, it was revealed that as temperature increased, the ionic conductivity monotonically increased, but electronic conductivity decreased. The same behaviour was also reported for the $La_{1-x}Sr_xCo_{1-y}Fe_yO_{3-\delta}$,[15] $Sr_{0.9}Ca_{0.1}Co_{0.89}Fe_{0.11}O_{3-\delta}$, $SrCoO_{3-\delta}$[21] and $Ln_{0.6}Sr_{0.4}CoO_{3-\delta}$ (Ln = La, Pr, Nd, Sm and Gd) electrodes.[56]

It is generally reported that the ionic conductivity of MIECs with perovskite structure is independent of oxygen

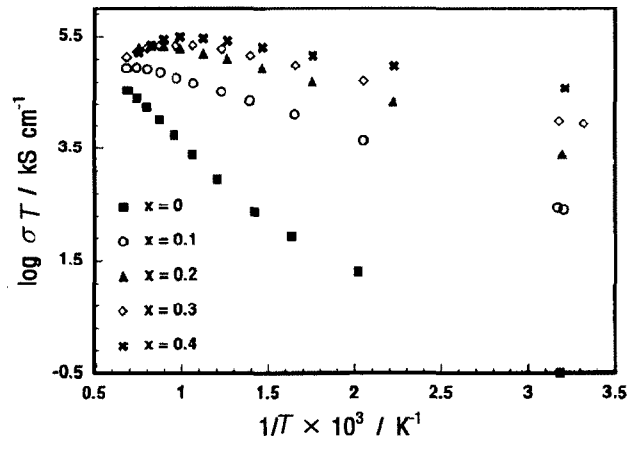

Fig. 3. Plots of the logarithmic σT versus the reciprocal of temperature obtained from the $La_{1-x}Sr_xCo_{0.2}Fe_{0.8}O_{3-\delta}$ electrodes with various Sr contents.[20]

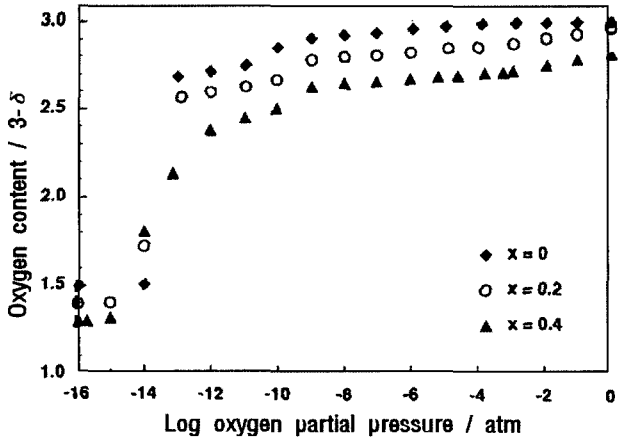

Fig. 4. Plots of the oxygen content versus logarithmic oxygen activity obtained from the $La_{1-x}Sr_xCo_{0.2}Fe_{0.8}O_{3-\delta}$ electrodes with various Sr contents.[15]

partial pressure p_{O_2}, since the concentration of extrinsic $V_O^{\cdot\cdot}$ induced by dopants is much higher than that of intrinsic $V_O^{\cdot\cdot}$. However, at very low p_{O_2}, the increase in intrinsic $V_O^{\cdot\cdot}$ concentration leads to the more deficiency of overall oxygen at electrode, and hence the ionic conductivity increases with decreasing p_{O_2}.

L.-W. Tai *et al.*[15] reported the oxygen content of mixed conducting $La_{1-x}Sr_xCo_{0.2}Fe_{0.8}O_{3-\delta}$ electrodes as a function of p_{O_2}. The dependence of oxygen deficiency on p_{O_2} for the $La_{1-x}Sr_xCo_{0.2}Fe_{0.8}O_{3-\delta}$ oxides with various Sr contents is shown in Fig. 4. As can be seen in Fig. 4, the oxygen deficiency remained nearly constant at high and medium p_{O_2} in the range of 1 to 10^{-10} atm, however, the oxygen content abruptly decreased at low p_{O_2} below 10^{-10} atm.

A.N. Petrov *et al.*[57] also investigated the dependence of electrical conductivity of $La_{0.7}Sr_{0.3}CoO_{3-\delta}$ electrode on p_{O_2} by TGA. From their work, it is noted that as p_{O_2} decreases, oxygen deficiency of $La_{0.7}Sr_{0.3}CoO_{3-\delta}$ electrode gradually increases, resulting in increase of ionic conductivity. On the other hand, the electronic conductivity decreases with increasing ionic conductivity. Since the contribution of ionic conductivity to the total electrical conductivity is negligibly small as compared with that contribution of electronic conductivity, the total electrical conductivity decreases with decreasing p_{O_2}. Recently, the electrical conductivity and oxygen deficiency of various MIECs as a function of p_{O_2} were investigated by D. Mantzavinos *et al*,[58] V.V. Kharton *et al.*[26,59] and M. Søgaard *et al.*[60]

3.2 Microstructural Property

As already mentioned in section 2, the characteristics of powders such as texture, purity, composition and homogeneity are crucially influenced by powder synthetic methods. At the same time, the initial powder properties strongly affect the geometrical properties of the resulting electrodes such as particle size, pore size and porosity under the same sintering condition. Accordingly, it is expected that the various synthetic methods largely affect the geometrical characteristics of the cathode which play an important role in the electrochemical behaviour of the electrode.

In general, it is suggested that the powder synthetic methods with combustion reaction produce the powders with smaller particle and homogeneous pore distribution than SSR method. L. Tan *et al.*[44] observed the influence of powder synthetic methods on microstructure of $Ba_{0.5}Sr_{0.5}Co_{0.8}Fe_{0.2}O_{3-\delta}$ membranes with perovskite structure. In their work, the grains of powders synthesised by Pechini method are connected together, while those of powders synthesised by SSR method are isolated. The particle size distributions of powders prepared by SSR and Pechini method are almost the same.

Fig. 5(a) and (b) depict the scanning electron microscopy (SEM) images of the cross-sectional $Ba_{0.5}Sr_{0.5}Co_{0.8}Fe_{0.2}O_{3-\delta}$ membranes prepared by SSR and Pechini methods under the same sintering condition, respectively.[44] It was found from Fig. 5 that $Ba_{0.5}Sr_{0.5}Co_{0.8}Fe_{0.2}O_{3-\delta}$ membranes showed the similar grain size of about 0.3–0.5 μm irrespective of powder synthetic method. On the other hand, the membrane prepared by Pechini method exhibited higher porosity and more homogeneous pore distribution as compared with that prepared by SSR method.

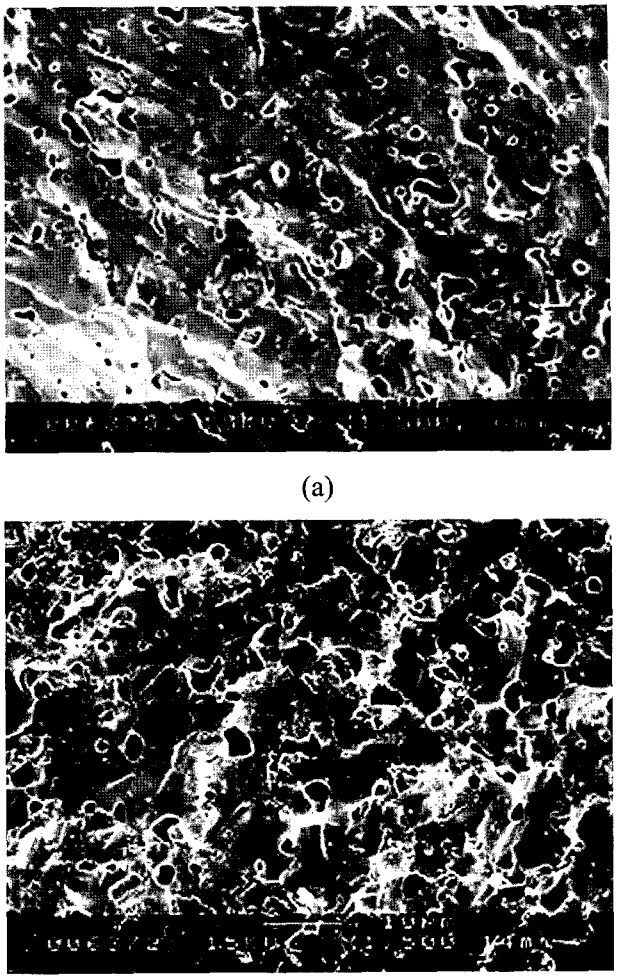

(a)

(b)

Fig. 5. Scanning electron microscopy (SEM) images of the cross section of $Ba_{0.5}Sr_{0.5}Co_{0.8}Fe_{0.2}O_{3-\delta}$ membranes prepared by (a) solid state reaction (SSR) and (b) Pechini methods sintered at 1373 K for 5 h in air.[44]

It is well known that the highly porous cathode for SOFC with mixed conductivity can facilitate the oxygen gas diffusion through the pores, but reduce the connectivity between particles, which impedes the electron and oxygen vacancy migrations. The porosity also affects the electrical properties of the electrode. Fig. 6 illustrates the electronic conductivity of $LaNi_{0.6}Fe_{0.4}O_3$ electrode as a function of porosity.[61] It is noted from Fig. 6 that the electrode with 3% porosity showed high electronic conductivity (580 S cm^{-1}), on the other hand, the electrode with 30% porosity had low electronic conductivity (257 S cm^{-1}). Since the electrode with higher porosity exhibits poorer connectivity between particles, the electronic conductivity decreases with increasing electrode porosity.

Recently, M. Bevilacqua *et al.*[62] reported that the electrical conductivity and morphology of electrodes are strongly affected by powder preparation method. In their work, the

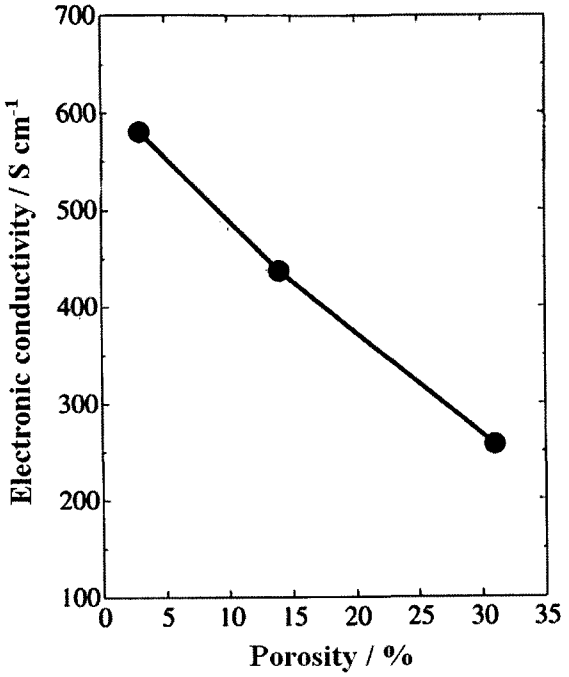

Fig. 6. Plots of the electronic conductivity versus porosity obtained from porous $LaNi_{0.6}Fe_{0.4}O_3$ electrode at 1073 K.[61]

porous mixed conducting $LaNi_{0.6}Fe_{0.4}O_3$ powders prepared by SG method showed better phase homogeneity than that prepared by GNP method. After sintering at 1373 K, BET surface areas of resulting electrodes prepared by GNP and SG methods are estimated to be 0.72 and 0.80 m^2 g^{-1} in value, respectively. From the above results, it is inferred that the electrode prepared by SG method exhibits higher porosity and more active sites for oxygen reduction reaction than that prepared by GNP method. Also, the electrical conductivities of $LaNi_{0.6}Fe_{0.4}O_3$ electrodes prepared by GNP and SG methods at 1373 K are calculated to be 250 and 300 S cm^{-1} in value, respectively. This is consistent with the results explained in Fig. 5.

4. Electrochemical Application of Mixed Conducting Oxides to Electrode Materials in Solid Oxide Fuel Cell (SOFC)

Let us consider the oxygen reduction reaction on the MIEC which generally holds the high concentration of oxygen vacancy. The mechanism of oxygen reduction on the porous MIEC is visualised in Fig. 7(a).[63] According to Fig. 7(a), it can tentatively be deduced that oxygen reduction is not restricted to the three phase boundaries (TPBs) among electrode, electrolyte and gas, but it is significantly extended from the origin of the TPBs into the electrode/gas interface segments due to its high ionic conductivity.

In general, it has been reported[64,65] that both the diffusion reaction of gaseous oxygen through the pores and the adsorption reaction of oxygen molecule on the electrode surface are too facile to affect oxygen reduction at $T > 1173$ K and $p_{O_2} > 0.01$ atm. Accordingly, for MIECs with high concentration of oxygen vacancy, we can expect that the overall oxygen reduction reaction on the electrode is split into the following two consecutive substeps: diffusion of oxygen vacancy through the electrode and subsequent electron exchange reaction between oxygen vacancies and gaseous oxygen (charge transfer reaction) at the electrode/gas interface.

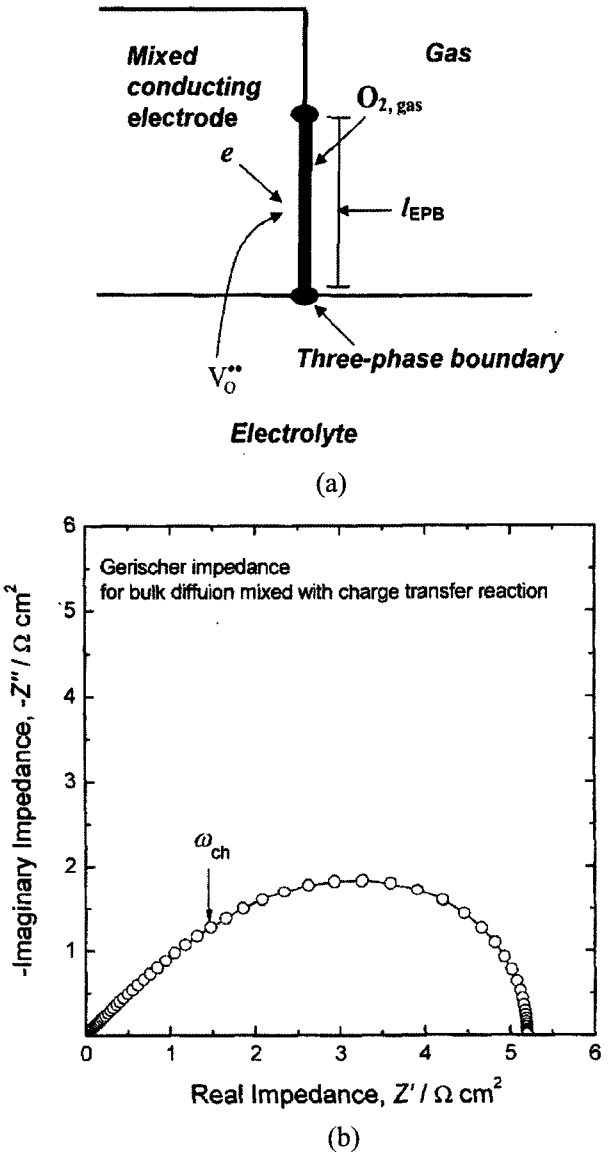

Fig. 7. (a) Schematic diagram of the diffusion reaction of oxygen vacancy and charge transfer reaction at the electrode/gas interface for mixed conducting electrode.[63] Here, l_{EPB} denotes the extended phase boundary length. (b) Nyquist plots of the ac-impedance spectrum[63] theoretically determined from Eq. (7) for bulk diffusion of oxygen vacancy and charge transfer reaction at the electrode/gas interface.

Under this circumstance, the theoretical ac-impedance model for the mixed conducting cathode developed by Adler *et al.*[64] can be analytically derived by considering the mixed diffusion and charge transfer reaction-controlled boundary condition. Solving Fick's diffusion equation by using Laplace transformation, the following electrode impedance $Z(\omega)$ is finally obtained.

$$Z(\omega) = R_{ch}\sqrt{\frac{1}{1+j\omega t_{ch}}} \quad (7)$$

$$\text{with } R_{ch} = \left(\frac{RT}{2F^2}\right)\sqrt{\frac{\tau_p}{(1-\varepsilon)c_{V_O^{\cdot\cdot}}D_{V_O^{\cdot\cdot}}A_s j_e}} \quad (8)$$

where R_{ch} designates the characteristic resistance [Ω cm^2] for the oxygen reduction reaction; A_s, the surface area of electrode per unit volume [cm^{-1}]; $cv_O^{\cdot\cdot}$, the oxygen vacancy concentration in the electrode [mol cm^{-3}]; t_{ch}, the characteristic time constant required for diffusion of oxygen vacancy from the electrode/gas interface through the electrode to the electrode/electrolyte interface [s]; ε, the porosity of electrode; $Dv_O^{\cdot\cdot}$, the pore tortuosity of electrode; τ_p, the component diffusivity of oxygen vacancy [cm^2 s^{-1}]; R, the gas constant [J mol^{-1} K^{-1}]; T, the absolute temperature [K]; j_e, the equilibrium exchange flux at $t=\infty$[mol cm^{-2} s^{-1}]; F, the faradaic constant [C mol^{-1}]; ω, the angular frequency [rad s^{-1}] and j represents the unit of the complex number ($\sqrt{-1}$).

Fig. 7(b) depicts the Nyquist plots of the ac-impedance spectrum theoretically determined from Eq. (7) for bulk diffusion of oxygen atom mixed with the charge transfer reaction at the electrode/gas interface with the values of T= 1273 K, $\tau_p = 2.5$, $\varepsilon = 0.3$, $cv_O^{\cdot\cdot} = 1.8 \times 10^{-3}$ mol cm^{-3}, $Dv_O^{\cdot\cdot} = 1 \times 10^{-5}$ cm^2 s^{-1}, $A_s = 1.5$ cm^{-1}, $j_e = 5.5 \times 10^{-6}$ mol cm^{-2} s^{-1} and $t_{ch} = 0.1$ s.[63] The ac-impedance spectrum exhibits a straight line inclined at a constant angle of 45° to the real axis at high frequencies, followed by an arc at low frequencies, which is frequently called the Gerischer behaviour.[64-66]

One can quantitatively analyse the kinetic parameters such as j_e and $Dv_O^{\cdot\cdot}$ which are of great importance for cathodic performance, by fitting the measured impedance spectra to Eq. (7). Actually, many researchers[64-68] have recently attempted to apply the models suggested by Adler to the interpretation of oxygen reduction reaction on the mixed conducting electrodes for SOFC. From the literatures,[64-68] the importance of j_e and $Dv_O^{\cdot\cdot}$ for the oxygen reduction mechanism on mixed conducting electrodes has been demonstrated at various values of T and p_{O_2}.

As a matter of fact, it is usually found that the ac-impedance spectrum for porous MIEC does not fairly coincide in shape with the Gerischer impedance. This inconsistency can be interpreted as the complexity of the microstructure of electrodes. The Gerischer impedance model for porous MIEC is assumed to be one-dimensional reaction and macro-homogeneous electrode, so the relationship between electrode performance and the microstructure of electrode is disregarded in the theoretical impedance model. Consequently, the occurrence of the deviation from the Gerischer impedance can be accounted for in terms of the inhomogeneities of the active reaction sites in the electrode due to the complex microstructure.

As already pointed out in section 3.2, the geometrical factors such as particle size, porosity and pore size are significantly influenced by powder synthetic methods. Thus, it is expected that the impedance spectra measured from the porous MIECs considerably vary in magnitude and shape depending upon the powder synthetic methods. For instance, in the case of mixed conducting electrodes prepared by SSR method such as $La_{0.9}Sr_{0.1}Co_{0.2}Fe_{0.8}O_{3-\delta}$ electrode, the measured impedance spectra significantly deviated from the Gerischer behaviour, as shown in Fig. 8. Fig. 8 illustrates the Nyquist plot of the impedance spectrum experimentally obtained from the porous $La_{0.9}Sr_{0.1}Co_{0.2}Fe_{0.8}O_{3-\delta}$ electrode synthesised by SSR method. In this case, considering that one can hardly prepare the fine and homogeneous powder using SSR method, this discrepancy may arise from the agglomeration and inhomogeneity of particle in the electrode.

On the other hand, it has been reported[33-40] that Pechini and GNP methods can provide the powders with fine and homogeneous particles and pores. For the electrode prepared by Pechini and GNP methods, the particles and pores are smaller in size than that prepared by SSR method, and they are homogeneously distributed and continuously connected each other through the electrode. In this case, oxygen gas can uniformly penetrate into the electrode, and hence the electrochemical-active sites for oxygen reduction reaction are widely distributed within the electrode.

Fig. 9(a) illustrates the Nyquist plots of the ac-impedance spectrum measured at 923 K in air from the porous $Sr_{0.8}Ce_{0.1}Fe_{0.7}Co_{0.3}O_{3-\delta}$ electrode synthesised by Pechini method.[69] The impedance spectrum is quite similar in shape to the Gerischer impedance, implying that the reaction sites are assumed to be homogeneously distributed. Furthermore, in spite of relatively lower measuring temperature, the magnitude of the overall impedance spectrum is smaller as compared with that spectrum in Fig. 8. This indicates that well-distributed small pores and particles facilitate gas transport and maximise surface area, which leads to larger electrochemical reaction sites for oxygen reduction. Thus, it is deduced that the polarisation resistance of porous MIEC can

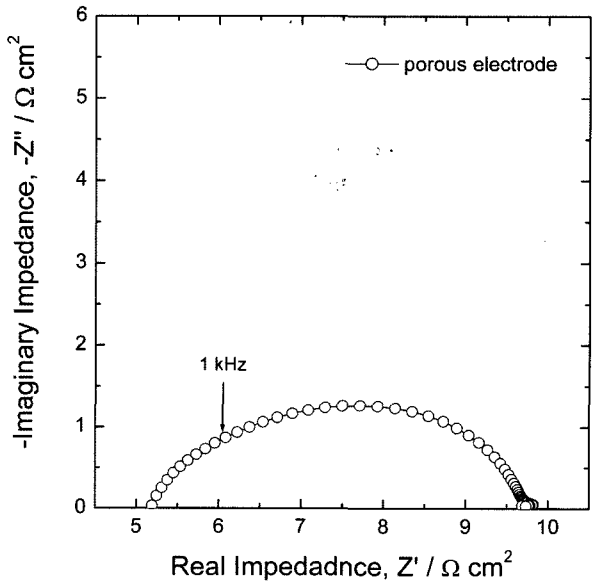

Fig. 8. Nyquist plot of the ac-impedance spectrum measured at 1023 K in air on the porous mixed conducting $La_{0.9}Sr_{0.1}Co_{0.2}Fe_{0.8}O_{3-\delta}$ electrode prepared by solid state reaction (SSR) method.

be decreased by a continuous microstructure and sufficient connection of grains.

J. Liu *et al.*[70] have attempted to illustrate the oxygen reduction reaction on the mixed conducting $La_{0.8}Sr_{0.2}Co_{0.8}Fe_{0.2}O_3$ electrode synthesised by SG method employing the ac-impedance spectroscopy. In their work, the electrode consisted of ultra fine particles with average particle size ranging from 2 to 4 μm and contained pores with diameters ranging from 0.2 to 2.0 μm. Fig. 9(b) depicts the Nyquist plot of the ac-impedance spectrum measured at 973 K in air on the porous $La_{0.8}Sr_{0.2}Co_{0.8}Fe_{0.2}O_3$ electrode.[70] Similar to the electrode synthesised by Pechini method, the impedance spectra follows the Gerischer behaviour. From the comparison of Fig. 8 with Fig. 9, it is suggested that the geometrical factors such as particle and pore sizes greatly influence the shape and value of the impedance spectra.

However, since there still remain uncertainty and disagreement about the oxygen reduction mechanisms of mixed conducting electrode, the impedance spectra observed from the porous MIECs synthesised by GNP or SG methods do not entirely resemble those predicted by the model of Adler.[64] In fact, the oxygen reduction kinetics can be also influenced by the properties of the electrode/electrolyte interface and surface composition.[71] Nevertheless, in most cases, it has been observed that the electrochemical performance is more sensitive to the microstructure of porous electrode than the other factors. Accordingly, in view of the geometrical characteristics, it is meaningful to correlate the powder synthetic methods to the electrochemical behaviour of porous electrode.

If we consider the dense mixed conducting electrode with well-defined structure, the effect of powder synthetic method on the electrochemical properties is negligibly small as compared with the porous electrode since the dense electrode makes it possible to simplify reaction pathways and disregard the effect of pore structure. Recently, in our laboratory, the oxygen reduction reaction on dense mixed conducting $La_{0.9}Sr_{0.1}Co_{0.2}Fe_{0.8}O_{3-\delta}$ electrode prepared by SSR method was investigated using ac-impedance spectroscopy.[72] Fig. 10 exhibits the Nyquist plot of the ac-impedance spectrum experimentally obtained from the dense mixed conducting $La_{0.9}Sr_{0.1}Co_{0.2}Fe_{0.8}O_{3-\delta}$ electrode at 1023 K in air.

It was found from Fig. 10 that the ac-impedance spectrum clearly showed the Warburg impedance at high frequencies associated with diffusion of oxygen vacancy, followed by an arc at low frequencies for the charge transfer reaction, similar to the Gerischer behaviour. It is noticeable that the ac-impedance spectrum in Fig. 10 is quite similar in shape to those spectra determined from dense $La_{0.7}Sr_{0.3}CoO_{3-\delta}$ electrode[73] prepared by radio frequency magnetron sputtering. This suggests that for dense electrodes the powder synthetic method has less effect on the electrochemical behaviour.

From the above results, it is recognised that the powder synthetic methods are of great importance for the microstructural properties of the resulting electrode such as particle size, porosity and the electrochemical-active sites, and hence have an impact on the kinetics of the oxygen reduction reaction. An extensive study on the effect of microstructural properties on the electrochemical behaviour is still under investigation in order to clarify the oxygen reduction mechanism on the porous mixed conducting cathode for SOFC.

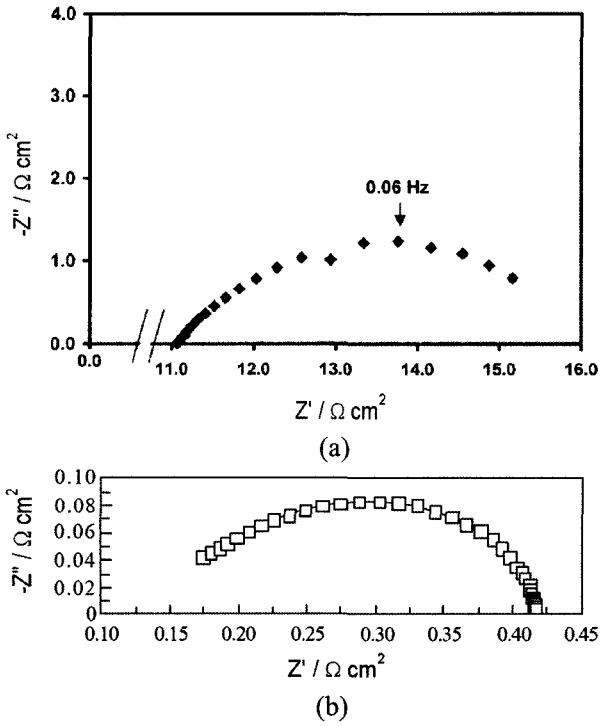

Fig. 9. Nyquist plots of the ac-impedance spectra (a) measured at 923 K in air on the porous $Sr_{0.8}Ce_{0.1}Fe_{0.7}Co_{0.3}O_{3-\sigma}$ electrode[69] prepared by Pechini method and (b) measured at 973 K in air on the porous mixed conducting $La_{0.8}Sr_{0.2}Co_{0.8}Fe_{0.2}O_3$ electrode[70] prepared by sol-gel (SG) method.

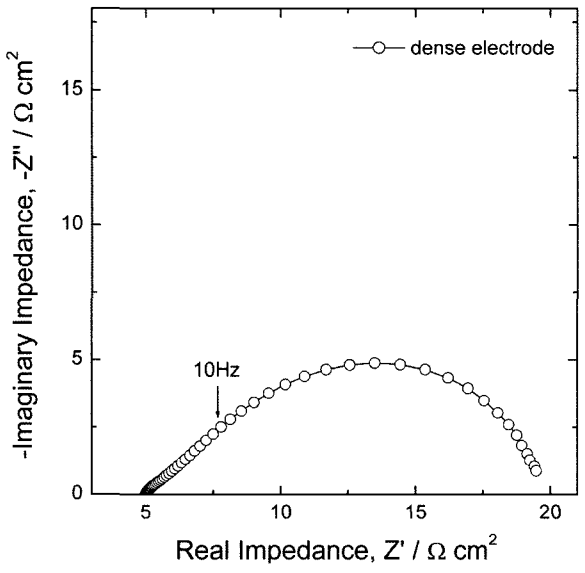

Fig. 10. Nyquist plots of the ac-impedance spectrum measured at 1023 K in air on the dense mixed conducting $La_{0.9}Sr_{0.1}Co_{0.2}Fe_{0.8}O_{3-\sigma}$electrode[72] prepared by solid state reaction (SSR) method.

Acknowledgements

This study was supported by a research No. N-FC12-P-03-3-010 for 5-year period 2004/2009 from "National RD&D Organization for Hydrogen & Fuel Cell" and "Ministry of Commerce, Industry and Energy". Furthermore, this work was partly supported by the Brain Korea 21 project.

Nomenclature

A_s	surface area of electrode per unit volume [cm^{-1}]
C	pre-exponential factor
$cv_O^{\cdot\cdot}$	oxygen vacancy concentration [mol cm^{-3}]
$Dv_O^{\cdot\cdot}$	component diffusivity of oxygen vacancy [cm^2 s^{-1}]
E_a	activation energy for conduction [eV]
EDS	energy dispersive spectroscopy
ε	porosity of electrode
F	faradaic constant [C mol^{-1}]
GNP	glycine nitrate process
j	unit of the complex number ($\sqrt{-1}$)
j_e	equilibrium exchange flux at $t=\infty$[mol cm^{-2} s^{-1}]
k	Boltzmann constant [eV K^{-1}]
l_{EPB}	extended phase boundary length
MIEC	mixed ionic/electronic conductor
p_{O_2}	oxygen partial pressure
R	gas constant [J mol^{-1} K^{-1}]
R_{ch}	characteristic resistance
SEM	scanning electron microscope
SG	sol-gel
σ	electrical conductivity [S cm^{-1}]
SOFC	solid oxide fuel cell
SSR	solid state reaction
T	absolute temperature [K]
t_{ch}	characteristic time constant required for diffusion of oxygen vacancy from the electrode/gas interface through the electrode to the electrode/electrolyte interface [s]
τ_p	pore tortuosity of electrode
TGA	thermogravimetric analysis
TPB	three phase boundary
TPD	temperature-programmed desorption
$V_O^{\cdot\cdot}$	oxygen vacancy
ω	angular frequency [rad s^{-1}]
XPS	X-ray photoelectron spectroscopy
XRD	X-ray diffraction

Reference

1. Y. Teraoka, H.-M. Zhang, S. Furukawa and N. Yamazoe, *Chem. Lett.*, **1985**, 1743 (1985).
2. Y. Teraoka, T. Nobunaga and N. Yamazoe, *Chem. Lett.*, **1988**, 503 (1998).
3. T. Ishihara, M. Honda, T. Shibayama, H. Minami, H. Nishiguchi and Y. Takita, *J. Electrochem. Soc.*, **145**, 3177 (1998).
4. M. Feng, J.B. Goodenough, K.Q. Huang and C. Milliken, *J. Power Sources*, **63**, 47 (2000).
5. A. Hartley, M. Sahibzada, M. Weston, I.S. Metcalfe and D. Mantzavinos, *Catal. Today*, **55**, 197 (2000).
6. F. Lecarpentier, H.L. Tuller and N. Long, *J. Electroceram.*, **5**, 225 (2000).
7. S.J. Skinner, *Fuel Cells Bull.*, **4**, 6 (2001).
8. Z. Shao and S.M. Halie, *Nature*, **431**, 170 (2004).
9. H. Kruidhof, H.J.M. Bouwmeester, R.H.E.v. Doorn and A.J. Burggraaf, *Solid State Ionics*, **63/65**, 816 (1993).
10. V.V. Kharton, A.P. Viskup, E.N. Naumovich and N.M. Lapchuk, *Solid State Ionics*, **104**, 67 (1997).
11. H. Kusaba, G. Sakai, N. Miura and N. Yamazoe, *Ionics*, **6**, 47 (2000).
12. J.E. ten Elshof, H.J.M. Boumeester and H. Verweij, *Appl. Catal.* A : General, **130**, 195 (1995).
13. H. Wang, Y. Cong and W. Yang, *Catal. Today*, **82**, 157 (2003).
14. Y. Takeda, Y. Sakaki, T. Ichikawa, N. Imanishi, O. Yamamoto, M. Mori, N. Mori and T. Abe, *Solid State Ionics*, **72**, 257 (1994).
15. L.-W. Tai, M.M. Nasrallah and H.U. Anderson, *J. Solid State Chem.*, **118**, 117 (1995).
16. J.W. Stevenson, T.R. Armstrong, R.D. Carneim, L.R. Pederson and W.J. Weber, *J. Electrochem. Soc.*, **143**, 2722 (1996).
17. V.V. Kharton, A.P. Viskup, D.M. Bochkov, E.N. Naumovich and O.P. Reut, *Solid State Ionics*, **110**, 61 (1998).
18. J. Mizusaki, J. Tabuchi, T. Matsuura, S. Yamauchi and K. Fueki, *J. Electrochem. Soc.*, **136**, 2082 (1989).
19. Y. Teraoka, T. Nobunaga, K. Okamoto, N. Miura and N. Yamazoe, *Solid State Ionics*, **48**, 207 (1991).
20. L.-W. Tai, M.M. Nasrallah, H.U. Anderson, D.M. Sparlin and S.R. Sehlin, *Solid State Ionics*, **76**, 273 (1995).
21. Z.Q. Deng, W.S. Yang, W. Liu and C.S. Chen, *J. Solid State Chem.*, **179**, 362 (2006).
22. J. Mizusaki, *Solid State Ionics*, **52**, 79 (1992).
23. J. Holc, D. Kuscer, M. Krovat, S. Bernik and D. Kolar, *Solid State Ionics*, **95**, 259 (1997).
24. H. Ullmann, N. Trofimenko, F. Tietz, D. Stöver and A. Ahmad-Khanolou, *Solid State Ionics*, **138**, 79 (2000).
25. M.V. Patrakeev, E.B. Mitberg, A.A. Lakhtin, I.A. Leonidov, V.L. Kozhevnikov, V.V. Kharton, M. Avdeev and F.M.B. Marques, *J. Solid State Chem.*, **167**, 203 (2002).
26. V.V. Kharton, J.C. Waerenborgh, A.P. Viskup, S.O. Yakovlev, M.V. Patrakeev, P. Gaczynski, I.P. Marozau, A.A. Yaremchenko, A.L. Shaula and V.V. Samakhval, *J. Solid State Chem.*, **179**, 1273 (2006).
27. H. Nagamoto, E. Shinoda and H. Inoue, *Ind. Eng. Chem. Res.*, **32**, 1790 (1993).
28. M.N. Rahaman, *Ceramic Processing and Sintering*, Chap. 1, Marcel Dekker, Inc., New York, 1995.
29. V.V. Kharton, A.P. Viskup, E.N. Naumovich, A.A. Tonoyan and O.P. Reut, *Mater. Res. Bull.*, **33**, 1087 (1998).
30. E. Maguire, B. Gharbage, F.M.B. Marques and J.A. Labrincha, *Solid State Ionics*, **127**, 329 (2000).
31. L. Tan, X. Gu, L. Yang, W. Jin, L. Zhang and N. Xu, *J. Membr. Sci.*, **212**, 157 (2003).
32. J.B. Smith and T. Norby, *Solid State Ionics*, **177**, 639 (2006).
33. M. Pechini, U.S. patent 3 330 797, July 11 (1967).
34. C.M. Ronconi and E.C. Pereira, *J. Appl. Electrochem.*, **31**, 319 (2001).
35. M. Mori and N.M. Sammes, *Solid State Ionics*, **146**, 301 (2002).
36. A.V. Rosario and E.C. Pereira, *Thin Solid Films*, **410**, 1 (2002).
37. M.C. Esteves, D. Gouvea and P.T.A. Sumodjo, *Appl. Surf. Sci.*, **229**, 24 (2004).
38. Y.-J. Yang, T.-L. Wen, H. Tu, D.-Q. Wang and J. Yang, *Solid State Ionics*, **135**, 475 (2000).
39. R. Peng, C. Xia, Q. Fu, G. Meng and D. Peng, *Mater. Lett.*, **56**, 1043 (2002).
40. R. Peng, X. Fan, Z. Jiang and C. Xia, *Fuel Cells*, **6**, 455 (2006).
41. R. Chiba, F. Yoshimura, Y. Sakurai, Y. Tabata and M. Arakawa, *Solid State Ionics*, **175**, 23 (2004).
42. P.G. Keech, D.E. Trifan and V.I. Birss, *J. Electrochem. Soc.*, **152**, A645 (2005).

43. F.J. Lepe, J. Fernández-Urbán, L. Mestres and M.L. Marínz-Sarrión, *J. Power Sources*, **151**, 74 (2005).
44. L. Tan, X. Gu, L. Yang, W. Jin, L. Zhang and N. Xu, *J. Membr. Sci.*, **212**, 157 (2003).
45. R.M. German, *Powder Metallurgy Science*, Chap. 5, Pennsylvania State University, New Jersey, 1994.
46. L.A. Chick, L.R. Pederson, G.D. Maupin, J.L. Bates, L.E. Thomas and G.J. Exarhos, *Mater. Lett.*, **10**, 6 (1990).
47. T.-L. Wen, H. Tu, Z. Xu and O. Yamamoto, *Solid State Ionics*, **121**, 25 (1999).
48. L. Qiu, T. Ichikawa, A. Hirano, N. Imanishi and Y. Takeda, *Solid State Ionics*, **158**, 55 (2003).
49. J. Gao, X. Liu, D. Peng and G. Meng, *Catal. Today*, **82**, 207 (2003).
50. J. Peña-Martínez, D. Marrero-López, D. Pérez-Coll, J.C. Ruiz-Morales and P. Núñez, *Electrochim. Acta*, **52**, 2950 (2007).
51. H.-R. Rim, S.-K. Jeung, E. Jung and J.-S. Lee, *Mater. Chem. Phys.*, **52**, 54 (1998).
52. M. B. Phillipps, N. M. Sammes and O. Yamamoto, *Solid State Ionics*, **123**, 131 (1999).
53. S. Lee, Y. Lim, E.A. Lee, H.J. Hwang and J.-W. Moon, *J. Power Sources*, **157**, 848 (2006).
54. G.Ch. Kostogloudis, N. Vasilakos and Ch. Ftikos, *J. Eur. Ceram. Soc.*, **17**, 1513 (1997).
55. A. Petric, P. Huang and F. Tietz, *Solid State Ionics*, **135**, 719 (2000).
56. K.T. Lee and A. Manthiram, *J. Electrochem. Soc.*, **153**, A794 (2006).
57. A.N. Petrov, O.F. Kononchuk, A.V. Andreev, V.A. Cherepanov and P. Kofstad, *Solid State Ionics*, **80**, 189 (1995).
58. D. Mantzavinos, A. Hartley, I.S. Metcalfe and M. Sahibzada, *Solid State Ionics*, **134**, 103 (2000).
59. V.V. Kharton, E.V. Tsipis, I.P. Marozau, A.P. Viskup, J.R. Frade and J.T.S. Irvine, *Solid State Ionics*, **178**, 101 (2007).
60. M. Søgaard, P.V. Hendriksen, M. Mogensen, F.W. Poulsen and E. Skou, *Solid State Ionics*, **177**, 3285 (2006).
61. R. Chiba, F. Yoshimura and Y. Sakurai, *Solid State Ionics*, **124**, 281 (1999).
62. M. Bevilacqua, T. Montini, C. Tavagnacco, G. Vicario, P. Fornasiero and M. Graziani, *Solid State Ionics*, **177**, 2957 (2006).
63. J.-S. Kim and S.-I. Pyun, *J. Kor. Electrochem. Soc.*, **8**, 106 (2005).
64. S.B. Adler, J.A. Lane and B.C.H. Steele, *J. Electrochem. Soc.*, **143**, 3554 (1996).
65. S.B. Adler, J.A. Lane and B.C.H. Steele, *J. Electrochem. Soc.*, **144**, 1884 (1997).
66. J.-S. Kim, S.-I. Pyun, J.-W. Lee and R.-H. Song, *J. Solid State Electrochem.*, **11**, 117 (2007).
67. S.B. Adler, *Solid State Ionics*, **111**, 125 (1998).
68. N. Grunbaum, L. Dessemond, J. Fouletier, F. Prado and A. Caneiro, *Solid State Ionics*, **177**, 907 (2006).
69. M.T. Colomer, B.C.H. Steele and J.A. Kilner, *Solid State Ionics*, **147**, 41 (2002).
70. J. Liu, A.C. Co, S. Paulson and V.I. Birss, *Solid State Ionics*, **177**, 377 (2006).
71. S.B. Adler, *Chem. Rev.*, **104**, 4791 (2004).
72. Y.-M. Kim, S.-I. Pyun, J.-S. Kim and G.-J. Lee, press in *J. Electrochem. Soc.*, **154** (2007).
73. A. Ringuedé and J. Fouletier, *Solid State Ionics*, **139**, 167 (2001).